ACS OMEGA

Open Access

http://pubs.acs.org/journal/acsodf

Article

Laser-Induced Graphene Strain Sensors for Body Movement Monitoring

Aida M. Barja, Yu Kyoung Ryu, Sandra Tarancón, Elena Tejado, Assia Hamada, Andres Velasco, and Javier Martinez*

Cite This: *ACS Omega* 2024, 9, 38359−38370

Read Online

ACCESS | Metrics & More | Article Recommendations | Supporting Information

ABSTRACT: To enable the development of artificial intelligence of things, the improvement of the strain sensing mechanisms and optimization of the interconnections are needed. Direct laser writing to obtain laser-induced graphene (LIG) is being studied as a promising technique for producing wearable, lightweight, highly sensitive, and reliable strain sensors. These devices show a higher degree of flexibility and stretchability when transferred to an elastomeric substrate. In this article, we manufactured polydimethylsiloxane (PDMS)-encapsulated LIG piezoresistive strain sensors with a quasi-linear behavior and a gauge factor of 111. The produced LIG was morphologically characterized via Raman spectroscopy and scanning electron microscopy before and after the electromechanical characterization and before and after the LIG transfer to PDMS. The results from these analyses revealed that the integrity of the material after the test was not affected and that the LIG volume in contact with the substrate increased after transfer and encapsulation in PDMS, leading to the improvement of the sensor performance. The sensors' capability for measuring bend angles accurately was demonstrated experimentally, making them useable in a wide range of applications for human body movement monitoring as well as for structural health monitoring. Regarding body monitoring, a PDMS-encapsulated LIG sensor for knee bending angle detection was proposed. This device showed unaffected performance of 1500 cycles under 8% uniaxial deformation and with response times in the range of 1−2 s

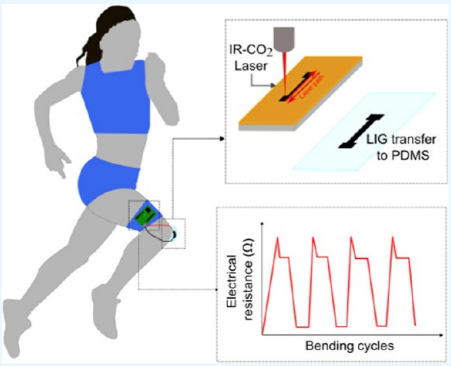

1. INTRODUCTION

In our current society, the technology industry is dominated by two main trends in continuous development and growth: the internet of things (IoT) and artificial intelligence (AI).[1] When IoT and AI work together it is called AI of things (AIoT), whose working principle consists of sensing stimulus, collecting and processing such data, and finally respond appropriately to the received stimulus.[2] To allow AIoT evolution, the development of lightweight, flexible, and wearable electronics is necessary, especially regarding strain sensing mechanisms that in most of the applications are attached to human body, clothes, or electronic devices carried by a person.[3−5] Furthermore, these strain sensors are required to possess a high sensitivity, a wide range of stretchability and deformability, a low hysteresis, and linear response as well as a fast responsiveness and a good stability. Moreover, low-cost and easy-to-manufacture devices are preferred. Conventional metallic strain gauges, though their low manufacturing cost, are not suitable for human body monitoring applications due to their limited sensitivity and stretchability:[6] generally, they cannot withstand strains above 5% before fracture[7] and do not return to their original position after deformation. Different materials are being studied as possible candidates for flexible strain sensors such as metal oxides, low dimensional nanostructures, including quantum dots and nanowires, and 2D materials like graphene and transition-metal dichalcogenides.[8−11] However, all these materials have to overcome yet different issues like limited sensitivity, low reliability, nonlinear response, and manufacturing challenges. Among them, graphene is one of the most studied materials for flexible sensors due to its outstanding electrical and mechanical properties:[12−14] electron mobilities up to 200.000 $cm^2/V\ s$,[15] an intrinsic strength of 130 MPa,[16] a Young's modulus of 1 TPa and a reversible strain of 25%.[17] Also, graphene piezoresistivity and its ability to work as a strain gauge has been demonstrated in different investigations.[18−20] In addition, graphene was employed as a heater skin in a recent work, due to its high heating efficiency and stability.[21]

Due to the high potential displayed by graphene and other low-dimensional carbon-based materials, several fabrication methods are being developed to manufacture them into

Received: November 14, 2023
Revised: August 11, 2024
Accepted: August 14, 2024
Published: August 30, 2024

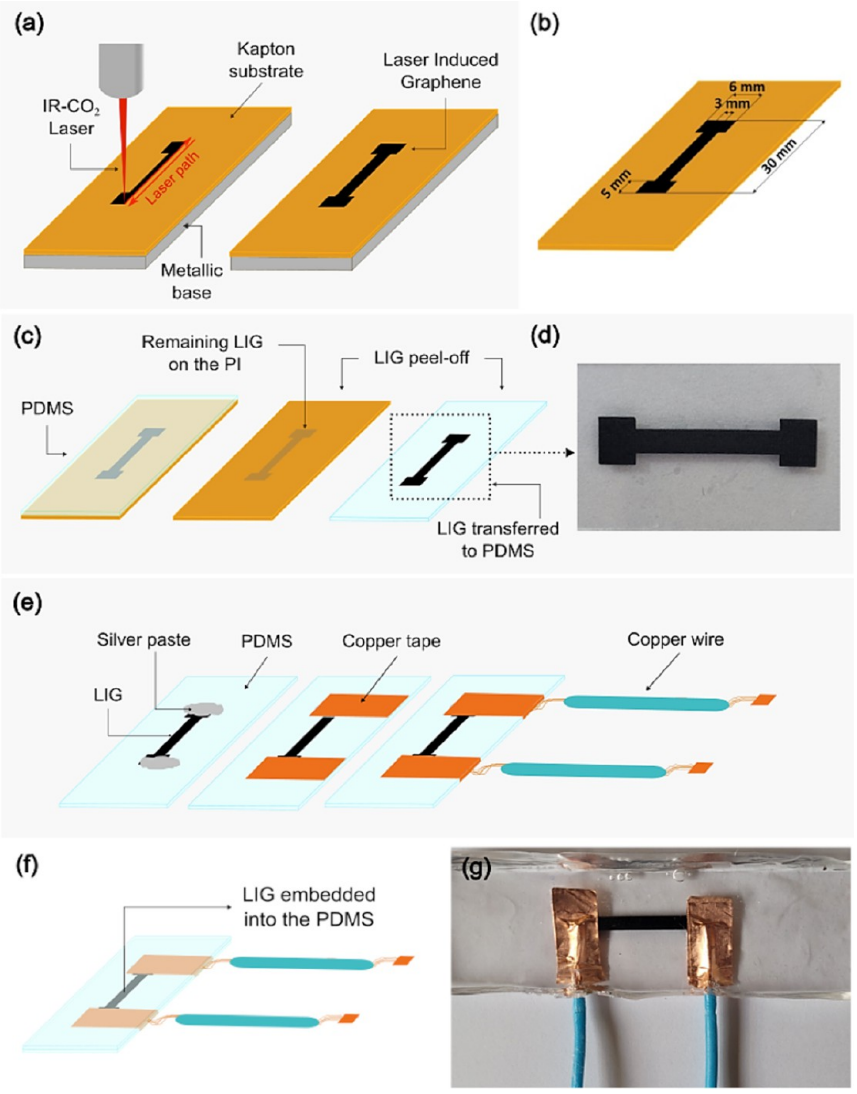

Figure 1. LIG on a PI substrate. (a) Scheme of the engraving process, showing the different elements involved and the print direction. (b) Scheme in which the dimensions of the designed and patterned LIG sensor are presented. (c) LIG transfer from PI to PDMS substrate, by LIG peel-off. (d) Real image of the LIG transferred to the PDMS sensor. (e) Scheme of the steps followed for the sensor electrode connections. (f) Scheme of the sensor embedded in the PDMS. (g) Real image of the sensor embedded in the PDMS.

wearable sensors for health monitoring applications. Among them, liquid-phase exfoliation constitutes a popular choice due to its low-cost and scalable characteristics.[22,23] Another manufacturing technique, which field is experiencing a strong growth during the last years, is direct laser writing (DLW) to produce laser-induced graphene (LIG).[24,25] DLW presents several advantages: it is a fast, single-step process that enables material transformation and device patterning at the same time. It constitutes a low-cost technique and it requires neither special supporting processes of pre- or post-treatment nor cleanroom equipment.[26] The typical precursor material used to produce LIG and the one chosen for this work was a polyimide (PI) polymer, commonly referred by its commercial name as Kapton.[27,28] In order to obtain flexible and stretchable graphene based wearable sensors, it is necessary to transfer the LIG to an elastomeric substrate because the maximum strain of PI before breaking is <3%, while the allowable strain of human skin is >13%.[29] Therefore, the LIG synthesized first on the PI substrate is generally transferred to a polydimethylsiloxane (PDMS) elastomer, which is thermally and chemically stable, physically robust and flexible, transparent, nontoxic and biocompatible, and suitable for biomedical and microelectromechanical systems applications.[7] Another similar technique that has been widely explored is laser reduced graphene oxide,[30,31] but it supposes an extra waste of time if compared with the LIG technique, in which the processes of graphene oxide preparation and spin coating are not needed.[32] In summary, due to all the aforementioned potential, LIG sensors embedded in the PDMS substrate for body monitoring are actively being researched.[7,12,13,33,34]

In this paper, we used the DLW technique to manufacture LIG piezoresistive strain sensors for tracking body movement. First, we synthesized a graphene-like material with the sensor geometry on a flexible PI film. Then, the LIG sensors were transferred and encapsulated in a PDMS elastomer. Through electromechanical characterization, we compared the performance of both the PI-substrate and PDMS-encapsulated LIG sensors to show how the sensibility of the sensor improved after being transferred to the elastomer. We correlated this result not only in terms of the better elastic properties of

https://doi.org/10.1021/acsomega.3c09067
ACS Omega 2024, 9, 38359−38370

PDMS over PI but also because there was a significant increase in the volume and quality of contact between the material (LIG) and the substrate (PDMS). A gauge factor (GF) of 111 was obtained for quasi-linear PDMS-encapsulated LIG sensors, and a GF of 7.5 was obtained for quasi-linear PI-substrate LIG sensors. Besides, scanning electron microscopy (SEM) analyses of the LIG before and after being tested under tensile stress as well as before and after being transferred to the PDMS substrate were performed to follow the morphology of the material at the different stages. Raman spectra showed well-defined D, G, and 2D peaks, characteristic of graphene, before and after the strain tests. Finally, a setup for the measurement of the knee bending angle using the PDMS-encapsulated LIG strain sensor has been proposed, which exhibited 1500 cycles under 8% of deformation without deviation and presented response times in the range 1−2 s.

2. EXPERIMENTAL SECTION

2.1. LIG Synthesis and Sensor Fabrication. For the transformation of the 125 μm thick PI film (DuPont, Kapton HN) into LIG, a commercially available, low-cost, and hobby-grade laser cutter was used. This laser cutter is equipped with a continuous wave infrared CO_2 laser of λ = 10.6 μm, a nominal power of up to 40 W, and a scan speed of up to 600 mm/s. The sensor design is created with vector image editing software (Inkscape). K40 Whisperer software is used to send the sensor designs to the laser, adjust different parameters of the laser scribing process, and control the movement of the laser nozzle in the "x" and "y" positions. The sensors are engraved in a direction parallel to the strain that will be applied in the subsequent tensile tests, based on the results obtained in,[33] as shown in Figure 1a. The dimensions of the sensor, specified in the scheme from Figure 1b, were chosen with the objective of having a sensor as small as possible but easy to handle in the manufacturing process and also to measure responses that were above the limit of detection determined by the available equipment.

The most important laser parameters, which are going to have a deep impact on the morphology of the resulting graphene, are the power P [W], the scanning speed u_x [mm/s], and the operational distance z [mm].[28,35] The linear laser energy density (LLED) [J/m] was suggested to be the key parameter to dictate the piezo resistivity in LIG sensors and to be directly related with its sensitivity,[36] whose formula is

$$\mathrm{LLED} = P/u_x \tag{1}$$

In this work, the laser power was set to P = 2.4 W and the laser speed to u_x = 60 mm/s, having consequently LLED = 400 J/m, based on a recent work from our group.[26] Another important parameter is the laser fluence F [J/cm^2] that measures the areal energy irradiated on the surface, whose formula is[26]

$$F = \frac{P}{u_x \cdot s} \cdot \frac{s}{d_y} \tag{2}$$

where "s" is the focus beam size and "d_y" is the y-line spacing, in our case, with a value of 100 and 75 μm, respectively. Hence, the laser fluence used for manufacturing the sensor was F = 53.3 J/cm^2. Regarding the operational distance "z", the sensors were manufactured at the focal distance.

Once the LIG strain gauge sensor was scribed on the PI substrate (Figure 1b), the next step consisted of the transfer of the obtained LIG from the PI film to the elastomeric substrate (Figure 1c) and, finally, in the encapsulation of the sensor. In this work, we have used a PDMS elastomer: SYLGARD 184 Silicone Elastomer (DOW) for the LIG transfer and sensor encapsulation processes. First, the PDMS solution was prepared by mixing the prepolymer and the cross-linking agent with a ratio of 10:1 for 5−10 min. The mixture was introduced in a vacuum chamber for 2 h in order to remove the air bubbles, following the example of.[37] Next, the LIG pattern on the PI substrate was fixed with double-sided tape on the bottom of an aluminum or Teflon mold. Subsequently, the PDMS mixture was manually poured into it, always using the same quantity. The uniformity and the thickness of the sensor were kept thanks to the constrictions defined by the dimensions of the mold. Then, the mold was introduced into vacuum for 3 h[33] in order to enhance the infiltration of PDMS into the interconnected channels of the LIG porous network[12] and facilitate the LIG transfer to the elastomer. After removing the mold from the vacuum, it was introduced in the oven for 2 h at 80 °C for the cross-linking of the PDMS.[38] In the literature, a wide range of PDMS curing time and temperature sets are available.[12,33,34,38−41] The election of 2 h at 80 °C in our process was found to be optimal in terms of not damaging the sensor connections and achieving a well cross-linked PDMS, with a nonsticky surface and easy to demold. One day after the PDMS curing, the sensor was unmolded, and the PDMS plus the LIG were peeled off from the PI. A real picture of the LIG transferred to PDMS is shown in Figure 1d.

In the next step, the connections between the LIG sensor ends and the copper wire electrodes were performed by using silver paste and copper tape[42,43] (Figure 1e). After the connections were made, the sensor was placed again in the mold. Subsequently, the PDMS solution was poured onto the sensor for the encapsulation process (Figure 1f). After another cycle of PDMS curing and demolding, the final device was obtained (Figure 1g).

2.2. Characterization. The surface morphology and microstructure of the LIG sensor before and after electro-mechanical test and before and after transferring it to PDMS were analyzed by SEM using the equipment Inspect TM F50 (FEI Company) at a voltage of 5 kV. Raman spectroscopy, with the equipment LabRam HR Evolution (Horiba, Japan), was performed to check the integrity of graphene on the PI substrate before and after the electromechanical test, using a λ = 532 nm, lens of ×10 magnification, ND filter of 50%, accumulation of 5, and an acquisition time of 20 s. The equivalent characterization with the graphene on the PDMS substrate was not possible with this Raman instrument due to the excessive background of the signal emitted by the elastomer. The electrical resistance without deformation of the LIG sensors was measured by applying a continuous current of 1 mA and registering the voltage output with a potentiostat/galvanostat system AUTOLAB PGSTAT204 (Metrohm, Switzerland) operating with the software NOVA. For the electromechanical characterization, the sensor was uniaxially stretched at a speed of 50 mm/min using a universal testing machine INSTRON 4411 (INSTRON, US). This speed was set at the beginning based on the standard for polyimide characterization under tensile strength because the first tested sensors were on the PI substrate. To enable comparison of the results, the same testing speed was used later for the sensors embedded in the PDMS.

https://doi.org/10.1021/acsomega.3c09067
ACS Omega 2024, 9, 38359−38370

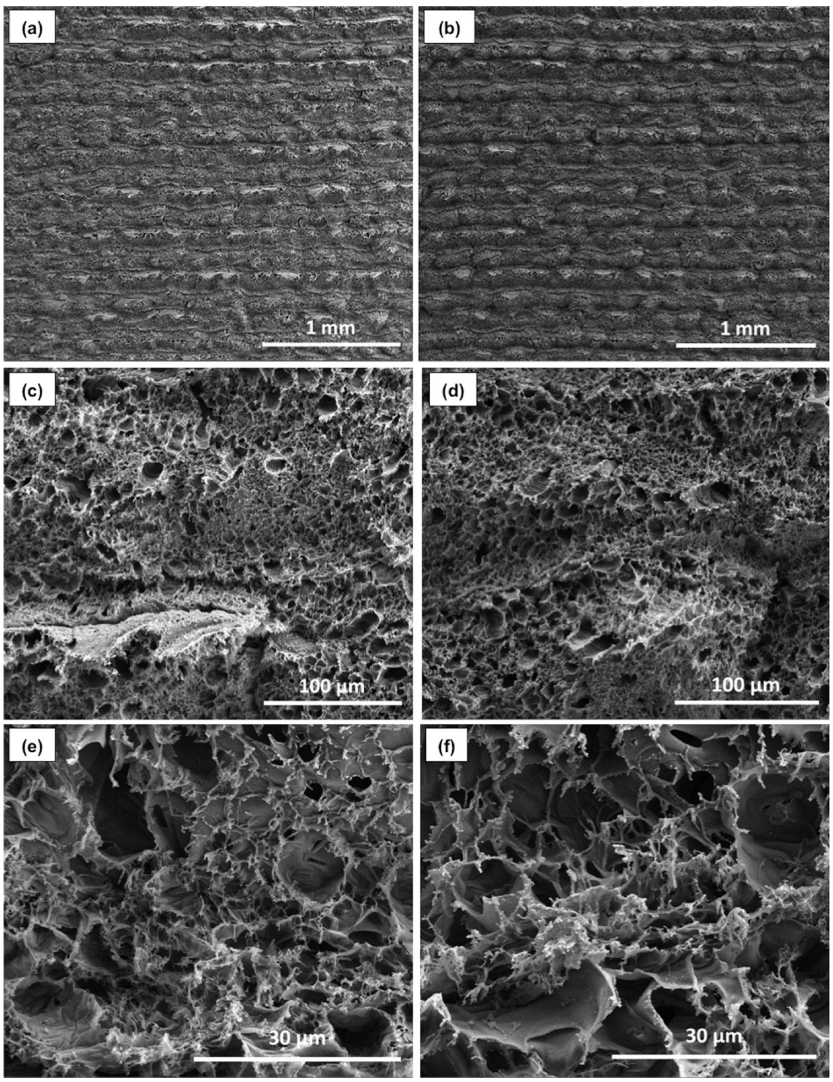

Figure 2. SEM images of the LIG morphology on the PI substrate sensor (a,c,e) before the strain tests and (b,d,f) after; at 100×, 1000×, and 5000× magnification, respectively.

To characterize the sensor sensibility (GF), a strain range of ε = 0−1.6% was applied. This strain range was decided based on the polyimide yield strength that corresponds to a strain value of 2%. Therefore, to ensure that the sensors on the PI substrate did not undergo permanent plastic deformation, we used a safe value limit of 1.6%. The same range was applied in the PDMS encapsulated sensors in order to compare the results. However, the full strain−stress curve of the PDMS sensor, obtaining a fracture strain of 21% was measured and is provided in Figure S1a (Supporting Information). The fracture under strain is produced at the edge of one of the connections, as shown in Figure S1b (Supporting Information). Therefore, the low value of the fracture strain is due to the current connections setup and not due to the PDMS elastomer or the LIG itself.

As measuring the response speed was not the objective, the position was maintained for 60 s on each strain value while applying a constant current of 1 mA, to give enough time to the sensor to stabilize after stretching it, hence measuring a more reliable resistance for each of the strains value. However, in the cyclability tests, the sensors were subjected to a strain range of ε = 0−8% because only PDMS encapsulated devices were tested and this material allows higher strain values with elastic recovering.[44] The sensor response speed was also assessed during the cyclability test, so the residence time on each strain value was only 3 s.

To estimate the sensor sensitivity, the GF was calculated, defined by the following equation[45]

$$\mathrm{GF} = \frac{\Delta R}{R_0}\cdot\frac{1}{\varepsilon} = \frac{R_\varepsilon - R_0}{R_0}\cdot\frac{1}{\Delta L/L_0} = \frac{R_\varepsilon - R_0}{R_0}\cdot\frac{1}{(L_\varepsilon - L_0)/L_0} \quad (3)$$

where R_0 is the electrical resistance of the sensor before applying a deformation, R_ε is the electrical resistance of the sensor after applying a strain ε, L_0 is the initial length of the sensor (before applying a deformation), and L_ε is the length of the sensor after applying a strain ε.

3. RESULTS AND DISCUSSION

3.1. Microstructure Characterization of the LIG Pattern. The LIG morphology on the PI substrate was analyzed before (Figure 2a,c,e) and after performing the electromechanical tests (Figure 2b,d,f) by SEM analysis for different magnifications (100×, 1000×, and 5000×). After the

https://doi.org/10.1021/acsomega.3c09067
ACS Omega 2024, 9, 38359−38370

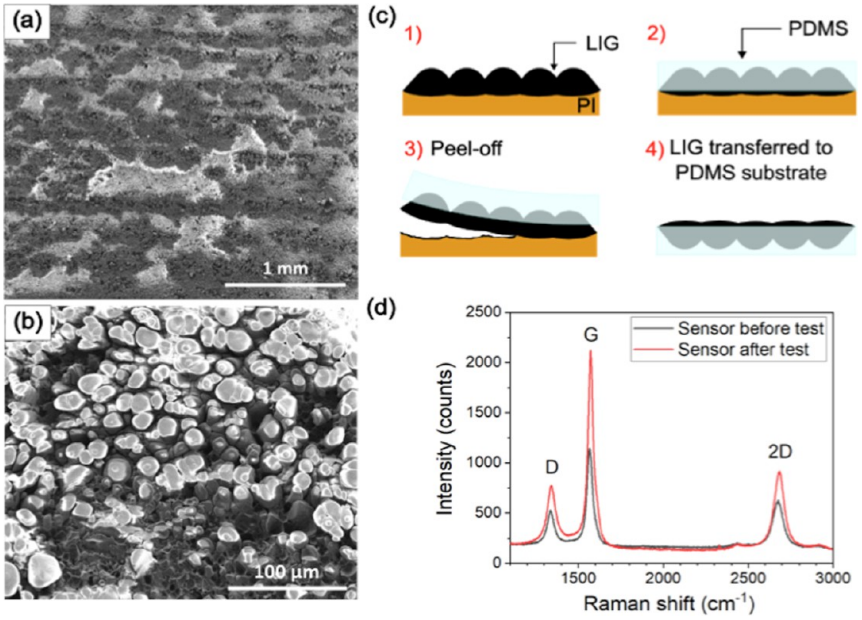

Figure 3. SEM image of the LIG after its transfer to PDMS (a) at 100× magnification and (b) at 1000× magnification. (c) Scheme representing how the LIG visible face looks like after PDMS transfer. (d) Raman spectra of the LIG sensor on PI before and after electromechanical characterization.

tests, the structure of graphene does not present cracks or distortions and remains very similar compared with before. This result indicates that the laser conditions used generate a robust and dense LIG film that keeps its integrity under deformation. In images at 100× magnification, the laser scribing direction can be easily observed (Figure 2a,b), as well as the mountain shape of each scribed path due to the thermal gradient during the lasing process.[33] For higher magnification at 1000×, the characteristic porous network of LIG does not seem to be broken after the tests (Figure 2d) compared with the microstructure before the tests (Figure 2c). Finally, from the images at 5000× magnification (Figure 2e,f), it can be observed that the LIG morphology consists of a hierarchical structure of interconnected multilayer flakes containing small and short fibers at their ends, with inhomogeneous pore sizes in the range of 2−14 μm. This morphology has already been observed in previous works on LIG from polyimide using a CO_2 laser.[46−48]

The LIG structure after its transfer to PDMS is also represented in the SEM images of Figure 3a,b. When PDMS is poured on the LIG grown in the PI substrate, the top part with the highest porosity is trapped on the elastomer. After the transfer process, the bottom part of the LIG film, which was in contact with the unmodified PI, is the one that protrudes from the PDMS (scheme represented in Figure 3c). In Figure 3a, the LIG structure appears flattened for two reasons: the bottom part was less porous, less modified[33] and due to the pressure exerted by the PDMS during the transfer process. However, the laser scribing direction can still be well noticed, corresponding the brightest regions to the center of the laser spot according to the volcanic shape of the LIG formation process that originates from the Gaussian laser energy distribution.[49] In the SEM image from Figure 3b, at a higher magnification, we observe that the LIG structure is continuous, namely, there still exists a good contact between the graphenic layers after the transfer process.

A characterization of the LIG on the PI substrate by Raman spectroscopy was performed in order to check that the graphenic nature was preserved after the straining experiments. In Figure 3d, the Raman spectra of the LIG sensor before and after the mechanical tests are represented. In these spectra, the characteristic peaks in graphene,[50,51] that is, peak D at 1340 cm^{-1}, peak G at 1573 cm^{-1}, and peak 2D at 2685 cm^{-1}, can be observed. Peak D is related with defects, peak G with the degree of graphitization, and peak 2D with the degree of crystallinity and arrangement of graphene monolayers.[52,53] One way of evaluating the LIG quality is by analyzing the I_D/I_G ratio, which gives an idea about the number of defects, degree of crystallinity, and graphitization;[54,55] and the I_{2D}/I_G ratio, which gives an idea about graphene quality, ordering, and number of layers.[56] For the sensor before the test, $I_D/I_G \approx 0.45$ and $\frac{I_{2D}}{I_G} \approx 0.53$. For the sensor after the test, $I_D/I_G \approx 0.37$ and $\frac{I_{2D}}{I_G} \approx 0.42$. These obtained intensity ratios indicate an acceptable defect number, decent crystallinity, that the produced graphene is multilayered, and that these ratios match with the literature values for LIG sensors.[33] The meaning of the observed differences regarding the center and the intensity of the D, G, and 2D peaks from the spectra before and after the tests cannot be analyzed because the area exposed by the laser spot in each case was not exactly the same. The LIG structure is inhomogeneous and to perform such analysis, a Raman spatial mapping or an average value from a significative sampling instead of single point measurements would be required.[26] However, this study was beyond the scope of this work.

3.2. Electromechanical Performance. First, we evaluate the electrical resistance without deformation of the sensors before and after the LIG transfer from the PI to the PDMS substrate to have a reference value and to see how the transfer affects the graphene electrical properties. The obtained values were R_0 = 85 Ω for the PI sensor and R_0 = 650 Ω for the PDMS sensor.

https://doi.org/10.1021/acsomega.3c09067
ACS Omega 2024, 9, 38359−38370

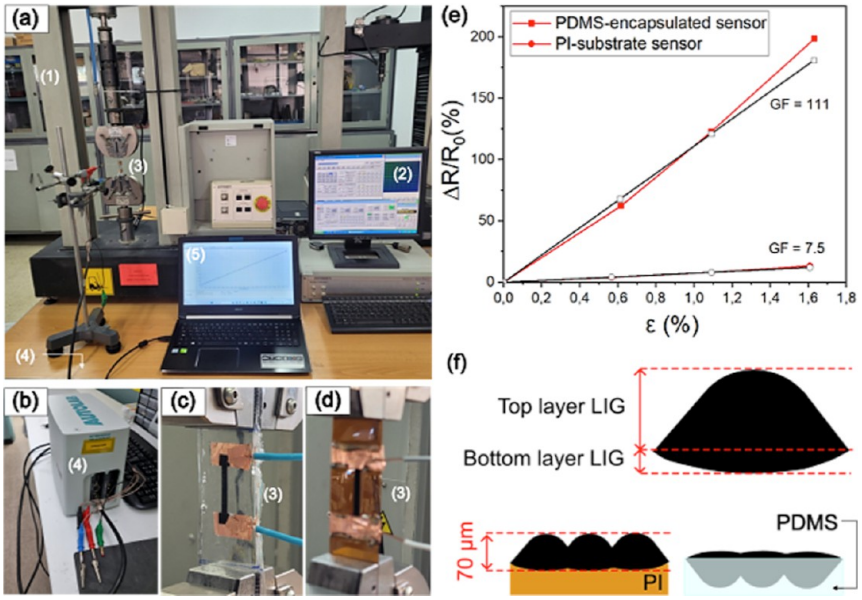

Figure 4. (a) Setup of the electromechanical characterization: (1) is the tensile mechanical testing machine, (2) is the computer to control the tensile testing machine, defining the deformation steps and the time maintained, (3) is the sensor, (4) is the potentiostat that applies a constant current to the sensor which is defined using the computer, and (5) in which also the voltage response of the sensor is registered. (b) Potentiostat/galvanostat AUTOLAB PGSTAT204 (Metrohm, Switzerland). (c) PDMS-encapsulated LIG strain sensor. (d) PI-substrate LIG strain sensor. (e) Comparison of the electromechanical characterization results for the PDMS-encapsulated LIG strain sensor and the PI-substrate LIG strain sensor. The red line represents the experimental results of the sensor, and the black line represents a fitting that represents a completely linear behavior using the average GF of the experimental results. (f) Scheme showing the influence of LIG transfer in the LIG specific area in contact with the substrate. Only a small LIG layer from the total grown thickness is embedded in the PI substrate and corresponds to worse quality, while when transferred to PDMS, more LIG, which corresponds to the top layer, is inside the elastomeric substrate and corresponds to better quality.

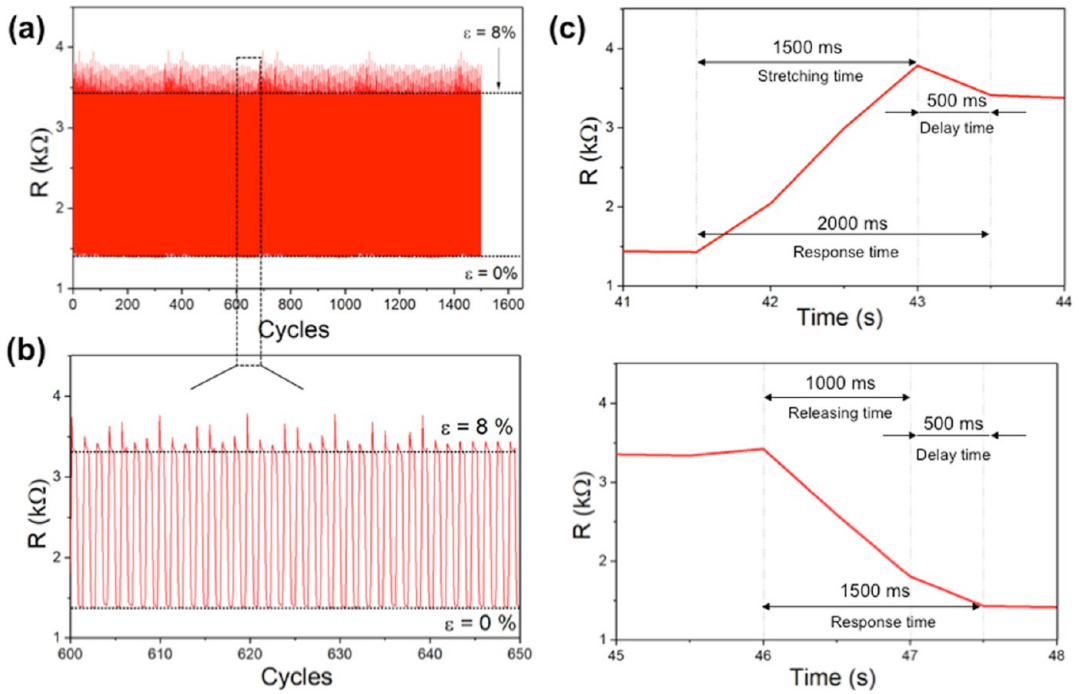

Figure 5. Long-term durability sensor characterization. (a) Resistance changes during the 1500 cycles of $\varepsilon = 0-8\%$. (b) Zoom in the graph (a) to show more clearly the repeatability between the peaks. (c) Response and delay time of the sensor during stretching (top) and releasing (bottom).

The setup used for the electromechanical characterization is shown in Figure 4a,b. A PDMS-encapsulated LIG strain sensor (Figure 4c) with quasi-linear behavior was obtained, showing an averaged GF of 111, Figure 4e. To demonstrate how the sensor sensibility improves when transferring the LIG to an elastomeric substrate, we manufactured and tested under uniaxial tensile strength a PI-substrate LIG sensor before transferring it to the elastomer (Figure 4d). As it was expected, the GF of the PI-substrate LIG sensor was 7.5, hence notably smaller than for the PDMS-encapsulated LIG strain sensor, as

https://doi.org/10.1021/acsomega.3c09067
ACS Omega 2024, 9, 38359−38370

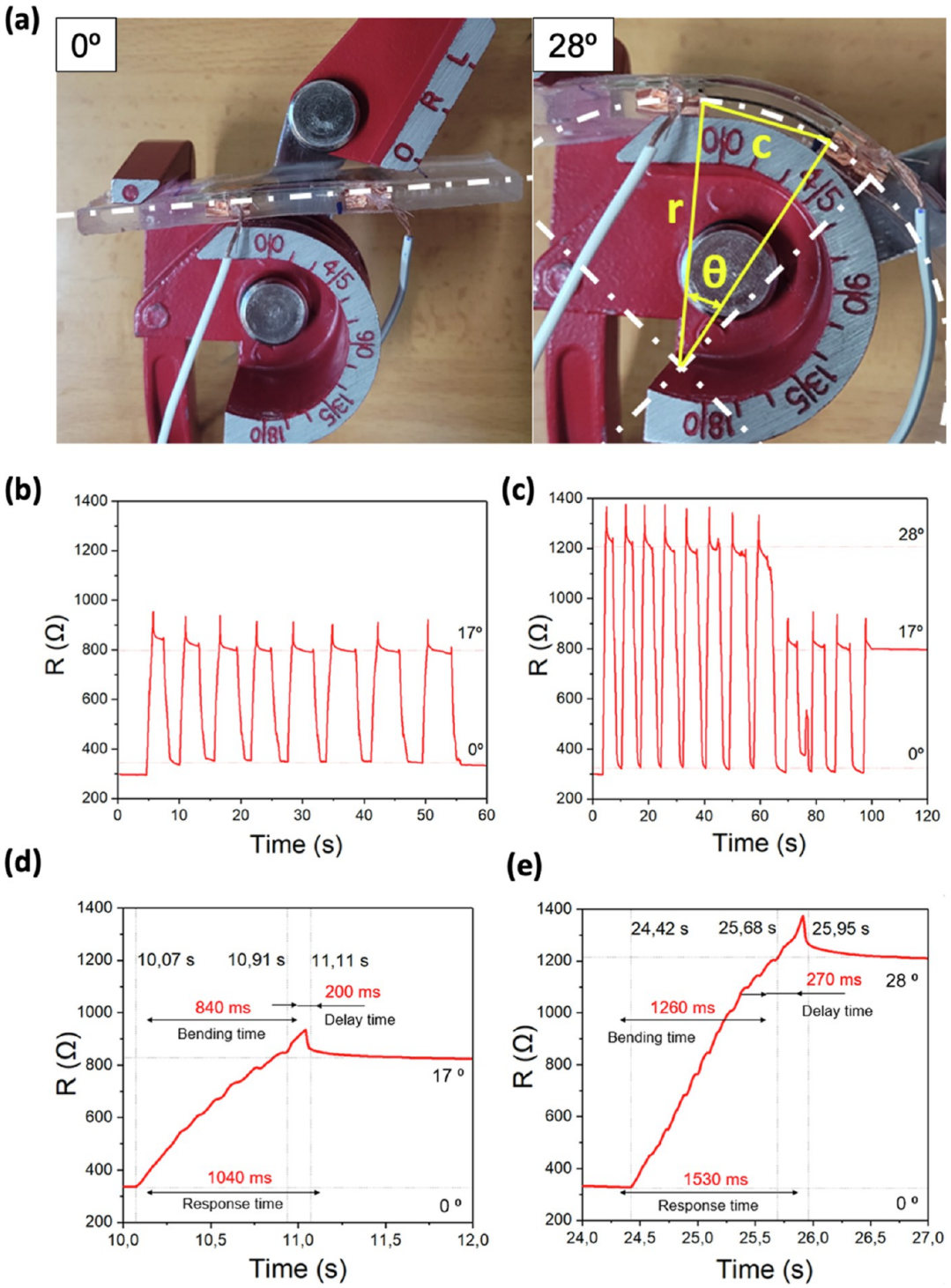

Figure 6. Demonstration of the LIG sensor for bending angle detection. (a) Device designed to bend the sensor to specific angles. In the left picture, the sensor is not bent, corresponding to 0°. In the right picture, it is highlighted how the measurements of the chord length "*c*" and the curvature radius "*r*" were taken to calculate the bend angle θ (case of a 28° bend angle). The curvature of the LIG under a bend angle can be well observed. (b) Experiment of 17° bend cycles (Movie S1). (c) Experiment of 28° bend cycles with a final transition to 17° (Movie S2). (d) Response time for 17° bend cycles. (e) Response time for 28° bend cycles.

observed in Figure 4e. The fact that the sensor sensibility (or GF) increases when transferring LIG to an elastomeric substrate (PDMS in this work) could be explained by means of the graphene specific surface area that is in contact with the substrate.[57] In the resulting LIG, we can differentiate between the top layer produced from the PI surface region and the bottom layer formed more deeply in the PI film. Hence, the top layer has enough space for expanding and a loose structure. However, the structure in the bottom layer has less porosity.[33] This microstructure difference results in a higher specific surface area for the top layer and hence a higher quality graphene. When the LIG is engraved on the PI substrate, the total thickness of the LIG is about 70 μm, being a smaller graphene percentage embedded in the PI[49] corresponding to

https://doi.org/10.1021/acsomega.3c09067
ACS Omega 2024, 9, 38359−38370

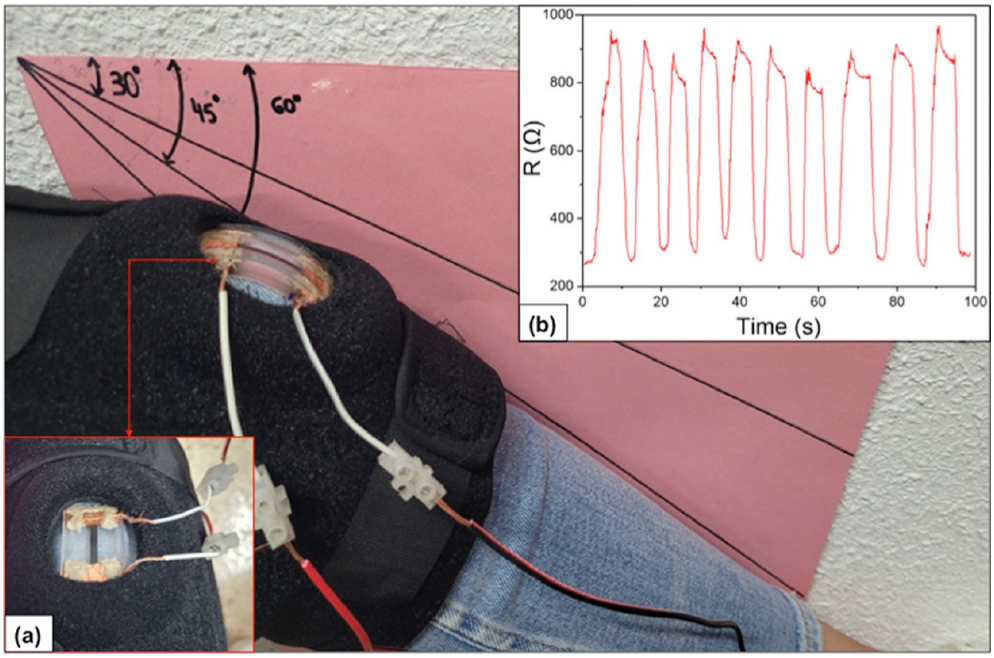

Figure 7. Setup of the sensor attached to a human knee in movement to demonstrate its applicability to human body monitoring. A knee pad was used to fix the sensor. (a) Zoom of the sensor front view. (b) Graph of the sensor's electrical response to bending cycles of 45°.

the bottom layer LIG. However, the remaining top layer and better-quality graphene remains outside the substrate and in contact with the atmosphere, not with the PI substrate. In contrast, when the LIG is transferred from the PI to the PDMS (scheme in Figure 3c), a higher quality graphene (corresponding to the top layer) and in a bigger volume is embedded in the elastomeric substrate, also resulting in a more continuous interconnected structure (microstructure in Figure 3b). Therefore, the volume of graphene in contact with the PDMS substrate is higher, having a greater ability to detect the substrate deformations, resulting in a higher GF of the sensor, Figure 4f. In addition, the sensors transferred to the PDMS were also encapsulated, so all of the LIG surface area is in contact with the substrate. Therefore, the graphene detects substrate deformation in all its faces, resulting in a higher GF.

To assess the long-term durability and stability of the LIG embedded in the PDMS sensor, it was subjected to 1500 cycles of ε = 0−8% uniaxial tensile deformation at a speed of 50 mm/min, maintaining 3 s on each position. During the cycles, a continuous current of 1 mA was applied while the voltage. In Figure 5a, there is the graph of the resistance change versus the different cycles, with the sensor showing neither damage nor change in behavior, clearly observed in the zoom from Figure 5b, and suggesting that it will be able to support more cycles without problems. Focusing on one of the cycles peaks, Figure 5c, we can measure the response time and delay time, following the example of,[33] being 2000 and 500 ms when stretching, and 1500 and 500 ms when releasing, respectively.

3.3. Demonstration of the LIG Strain Sensor for Bending Angle Detection. To demonstrate the applicability of the manufactured sensors for any question that involves measuring bend angles, a mechanism that allows control with exactitude of the bend angle of the sensor was designed, and the PDMS sensor was tested for cycles of 17 and 28°. The designed setup is shown in Figure 6a (left picture), where the sensor is not bent, equivalent to 0° angle state. To calculate the bend angle θ, the following relation with the chord length c and the curvature radius r was used, as reported in[58]

$$\sin\left(\frac{\theta}{2}\right) = \frac{c}{2 \cdot r} \tag{4}$$

θ, c, r, and the bending curvature of LIG are outlined in Figure 6a (right picture) for the case of the 28° angle.

In Figure 6b,c, the graphs of the sensor resistance response for cycles of bending under 17 and 28° are shown, respectively. In Figure 6c, the subsequent transition from a bending angle of 28 to 17° was applied. The cycles of bending under 17° shown in Figure 6b,c, performed in two different experiments, show a very similar resistance response, indicating the consistency of the fabricated sensors. The videos of the corresponding experiments of Figure 6b,c are shown in Movie S1 and Movie S2, respectively (Supporting Information). Focusing on one of the peaks, the response time for the cycles of 17° (Figure 6d) and for the cycles of 28° (Figure 6e) can be estimated, which were 1040 and 1530 ms, respectively. The difference is due to the bending time needed for the different angles, at not-controlled velocities because the sensors were manually bent. Anyway, the delay time of the sensor in both cases is around 200 ms and therefore considerably smaller than for the tensile strain cycles (Figure 5c). This result indicates that the sensor behaves better under bending deformations than under tensile deformations, at least in terms of response speed, as a function of how differently the LIG morphology is modified under angle bending vs under stretching.

The manufactured sensors are able to measure bend angles due to the piezoresistive effect; for the same reason, they are able to measure tensile strains. In both cases, the morphological changes on the LIG microstructure due to the applied deformation cause changes in the electrical resistance of the device.

3.4. Applicability of the Sensor for Human Body Monitoring. To test the applicability of the sensor to body movement monitoring, it was attached to a human knee in

https://doi.org/10.1021/acsomega.3c09067
ACS Omega 2024, 9, 38359−38370

Table 1. Figures of Merit and Type of Tests Performed on the Sensor of This Work and Other Similar Works from the Literature Are Depicted[a]

sensor materials	GF	cyclability tests (number of cycles)	bend angle tests	delay time (ms)	response time (ms)	refs
LIG in PDMS	GF = 160 ε = 0−1.8%	200 ε = 1,3,7%	no	negligible	70	7
LIG in PDMS	GF = 495 (n.l.) ε = 17−25%	12 000 ε = 4%	24−35−42°	no	250	12
LIG in PDMS	GF = 41 (n.l.) ε = 30−46%	3000 ε = 20%	no	no	287	13
LIG in PDMS	GF = 15.8 (n.l.) ε = 10−20%	2000 ε = 5%	no	1163	160	33
LIG in PDMS	GF = 43 (n.l.) ε = 45−48%	5000 ε = 20%	0−15−45−75−90°	no	300	42
LIG in PDMS	GF = 111 ε = 0−1.6%	1500 ε = 8%	0−17−28°	200	1040	this work

[a]Below the values of the GF and the number of cycles, the (range of) strain ε under which the measurements were done are provided. The abbreviation n.l. means nonlinear behavior of the sensor.

movement by using the setup shown in Figure 7. The sensor was attached to the volunteer's knee using a knee pad with a hole in the middle, which enabled the connection between the sensor and the potentiostat/galvanostat electrodes through cables. Then, the instrument supplied an electrical current while the knee was bent and subsequently, the changes in the electrical signal representing the sensor response were captured in a computer using the software NOVA.

The knee was bent in cycles of 45° while a constant current of 1 mA was applied and the voltage was registered to calculate the electrical resistance response of the sensor. The figure also shows a zoom of the sensor front view (a) and the graph of the sensor electrical response for bending cycles of 45° (b).

A proposed wearable device to carry on any joint would consist of a little power supply system, a data collection system, and an electrical resistance to deformation transducer. The power supply needs a capability of 1.2 V (or 1 mA), so a small battery or even a mini solar panel connected to the sensor electrodes could be used. The transduced data could be shown on a screen or used to communicate with a machine, robot, or a videogame to reproduce the human movements or to analyze them. The development of this wearable device opens up a huge number of possible applications, not only for human body monitoring but also for structural health monitoring. Specifically, it has an excellent potential in aerospace because it is lightweight, it presents an outstanding mechanical flexibility, and it could easily take the energy that needs to work from the solar panels typically placed in the space systems, constituting a self-powered unit.

3.5. Analysis of the Device Performance. In order to evaluate the performance of our proposed strain gauge sensor, we provide a comparison with other similar strain gauge sensors made of LIG embedded in PDMS from recent works found in the literature. The results are presented in Table 1. The GF value of the sensor fabricated in this work, of 111, falls within the range of values achieved by the other sensors. Concretely, compared to the sensors from refs 13 and 33 and,[42] the value of the GF of our sensor is higher, having used a smaller value of strain. Furthermore, our fabrication process has led to a device that presents a quasi-linear behavior, in contrast to the generally observed nonlinearity (n.l.). The result of the cyclability test of our sensor shows once more that its stability and reproducibility are good and akin to the values from the other works. In the case of the delay and response times, their values are going to depend on several factors such as the type of test performed on the sensor (tensile or bending load) and the strain rate, making more cumbersome the establishment of a fair comparison between the different devices

Regarding the use of LIG to fabricate piezoresistive strain sensors, this material has great potential to be implemented in real-life applications. Most of the commercial strain gauges, generally made of metals, present a GF in the range of 1−3, an applicable strain up to 5% and are quite brittle.[59−61] On the other hand, strain gauges that are based on silicon, which is a semiconductor, present a GF in the range of 20−40, but do not withstand strains above 0.3% due to the rigidity of the sensing material.[62] However, as can be observed from Table 1, LIG can supply a much higher range of strains and gauge factors. These results, together with its outstanding mechanical flexibility and lightweight characteristics, make LIG an attractive candidate for wearable electronics applications, such as body movement and health monitoring. Finally, in terms of production costs, LIG can be competitive. First, many of the used precursors to synthesize the material are low-cost plastics or organic materials. Then, the lasers that pyrolyze the precursors to generate LIG are either commercial hobby grade machines or are part of setups used for other characterization and fabrication techniques in industry/academic research.

4. CONCLUSIONS

In this work, we have manufactured strain gauge sensors using a low-cost, easy, and commercially available DLW technique to obtain LIG. PDMS-encapsulated LIG strain sensors with quasi-linear behavior and a GF of 111 were obtained. The influence of the LIG transfer on the sensor sensibility (or GF) was studied, testing a PI-substrate LIG strain sensor that showed a GF of only 7.5. The durability of the PDMS-encapsulated LIG strain sensors was tested subjecting the sensor to 1500 cycles of ε = 8%, and no deviation were observed in the sensor behavior during the cycles. Then, the sensor was subjected to bending cycles of 17 and 28°, showing a stable and repeatable response with an acceptable response time. Therefore, the sensor's ability to measure the bending angle was demonstrated. Its applicability for body movement monitoring was tested by fixing the sensor to a human knee in motion.

In summary, we have developed a wearable, flexible, lightweight, sensitive, and reliable strain sensor based on LIG and PDMS. The obtained sensor is able to measure bend angles accurately and would be easily implemented in a portable monitoring system with low energy requirements after further miniaturization. Therefore, many possible applications regarding human body movement monitoring have opened, for both body tracking and human−machine interaction. Furthermore, these sensors could be applied for structural health monitoring in critical aerospace structures.

https://doi.org/10.1021/acsomega.3c09067
ACS Omega 2024, 9, 38359−38370

■ ASSOCIATED CONTENT

Supporting Information

The Supporting Information is available free of charge at https://pubs.acs.org/doi/10.1021/acsomega.3c09067.

Stress−strain curve of the sensor (PDF)

Experiment of 17° bend angles monitored in real time (MP4)

Experiment of the transition from 28° bend angles to 17° bend angles monitored in real time (MP4)

■ AUTHOR INFORMATION

Corresponding Author

Javier Martinez − *Instituto de Sistemas Optoelectrónicos y Microtecnología, Universidad Politécnica de Madrid, Madrid 28040, Spain; Departamento de Ciencia de Materiales-CIME, E.T.S.I de Caminos, Canales y Puertos, Universidad Politécnica de Madrid, Madrid 28040, Spain;* orcid.org/0000-0002-5912-1128; Email: javier.martinez@upm.es

Authors

Aida M. Barja − *Instituto de Sistemas Optoelectrónicos y Microtecnología, Universidad Politécnica de Madrid, Madrid 28040, Spain;* orcid.org/0009-0007-5496-1631

Yu Kyoung Ryu − *Instituto de Sistemas Optoelectrónicos y Microtecnología, Universidad Politécnica de Madrid, Madrid 28040, Spain; Departamento de Física Aplicada e Ingeniería de Materiales, E.T.S.I Industriales, Universidad Politécnica de Madrid, 28006 Madrid, Spain;* orcid.org/0000-0002-5000-2974

Sandra Tarancón − *Departamento de Ciencia de Materiales-CIME, E.T.S.I de Caminos, Canales y Puertos, Universidad Politécnica de Madrid, Madrid 28040, Spain*

Elena Tejado − *Departamento de Ciencia de Materiales-CIME, E.T.S.I de Caminos, Canales y Puertos, Universidad Politécnica de Madrid, Madrid 28040, Spain;* orcid.org/0000-0002-5240-6702

Assia Hamada − *Instituto de Sistemas Optoelectrónicos y Microtecnología, Universidad Politécnica de Madrid, Madrid 28040, Spain*

Andres Velasco − *Instituto de Sistemas Optoelectrónicos y Microtecnología, Universidad Politécnica de Madrid, Madrid 28040, Spain; Departamento de Ingeniería Electrónica, E.T.S.I de Telecomunicación, Universidad Politécnica de Madrid, Madrid 28040, Spain;* orcid.org/0000-0003-4517-2415

Complete contact information is available at: https://pubs.acs.org/10.1021/acsomega.3c09067

Notes

The authors declare no competing financial interest.

■ ACKNOWLEDGMENTS

A.V. is in receipt of an FPU grant from the Spanish Government (FPU18/03235), funded by MCIN/AEI/10.13039/501100011033 "ESF Investing in your future". A.V., Y.K.R., and J.M. acknowledge the funding under project REGRAP-2D (PID2020-114234RBC22), which was funded by MCIN/AEI/10.13039/501100011033. Funding was also obtained from the Comunidad de Madrid through project NMAT2D-CM (P2018/NMT-4511) and MINCIN y Comunidad de Madrid, "Materiales Disruptivos Bidimensionales (2D)" (MAD2D-CM)-UPM1. Additional support from the Spanish "Agencia Estatal de Investigación" under the call "Proyectos de Generación de Conocimiento 2022" (3DPOS-THERMEC, PID2022-137274NB-C33PID) is also acknowledged. The authors also would like to acknowledge ICTS Micronanofabs.

■ REFERENCES

(1) Osifeko, M. O.; Hancke, G. P.; Abu-Mahfouz, A. M. Artificial Intelligence Techniques for Cognitive Sensing in Future IoT: State-of-the-Art, Potentials, and Challenges. *J. Sens. Actuator Netw.* **2020**, *9*, 21.

(2) Zhang, J.; Tao, D. Empowering Things with Intelligence: A survey of the progress, challenges, and opportunities in artificial intelligence of things. *IEEE Internet Things J.* **2021**, *8* (10), 7789−7817.

(3) Lu, Y.; Yang, G.; Wang, S.; Zhang, Y.; Jian, Y.; He, L.; Yu, T.; Luo, H.; Kong, D.; Xianyu, Y.; Liang, B.; Liu, T.; Ouyang, X.; Yu, J.; Hu, X.; Yang, H.; Gu, Z.; Huang, W.; Xu, K. Stretchable graphene-hydrogel interfaces for wearable and implantable bioelectronics. *Nat. Electron.* **2023**, *7* (1), 51−65.

(4) Wu, P.; Yiu, C. K.; Huang, X.; Li, J.; Xu, G.; Gao, Y.; Yao, K.; Chow, L.; Zhao, G.; Yang, Y.; Jiao, Y.; Yu, X. Liquid metal-based strain-sensing glove for human-machine interaction. *Soft Sci.* **2023**, *3* (4), 35.

(5) Yue, Y.; Li, X.; Zhao, Z.; Wang, H.; Guo, X. Stretchable flexible sensors for smart tires based on laser-induced graphene technology. *Soft Sci.* **2023**, *3* (2), 13.

(6) Bolton, W. Instrumentation System Elements. In *Instrumentation and Control Systems*, 3rd ed.; Bolton, W., Ed.; Newnes, 2021; pp 17−70.

(7) Jeong, S.-Y.; Ma, Y.-W.; Lee, J.-U.; Je, G.-J.; Shin, B.-S. Flexible and Highly Sensitive Strain Sensor Based on Laser-Induced Graphene Pattern Fabricated by 355 nm Pulsed Laser. *Sensors* **2019**, *19* (22), 4867.

(8) Han, S.; Peng, H.; Sun, Q.; Venkatesh, S.; Chung, K.; Lau, S. C.; Zhou, Y.; Roy, V. a. L. An overview of the development of flexible sensors. *Adv. Mater.* **2017**, *29* (33), 1700375.

(9) Han, F.; Li, M.; Ye, H.; Zhang, G. Materials, electrical performance, mechanisms, applications, and manufacturing approaches for flexible strain sensors. *Nanomaterials* **2021**, *11* (5), 1220.

(10) Jiang, H.; Zheng, L.; Liu, Z.; Wang, X. Two-dimensional materials: From mechanical properties to flexible mechanical sensors. *InfoMat* **2020**, *2* (6), 1077−1094.

(11) Yoon, Y.; Truong, P. L.; Lee, D.; Ko, S. H. Metal-Oxide nanomaterials synthesis and applications in flexible and wearable sensors. *ACS Nanosci. Au* **2022**, *2* (2), 64−92.

(12) Chhetry, A.; Sharifuzzaman, Md.; Yoon, H.; Sharma, S.; Xuan, X.; Park, J. Y. MOS2-Decorated Laser-Induced Graphene for a highly sensitive, hysteresis-free, and reliable piezoresistive strain sensor. *ACS Appl. Mater. Interfaces* **2019**, *11* (25), 22531−22542.

(13) Zheng, H.; Wang, H.; Yi, K.; Lin, J.; Chen, A.; Chen, L.; Zou, Z.; Liu, M.; Ji, Y.; Dong, L.; Lin, Z. Wearable LIG Flexible Stress Sensor based on Spider Web Bionic structure. *Coatings* **2023**, *13* (1), 155.

(14) Velasco, A.; Ryu, Y. K.; Boscá, A.; Ladrón-de-Guevara, A.; Hunt, E.; Zuo, J.; Pedrós, J.; Calle, F.; Martinez, J. Recent trends in graphene supercapacitors: from large area to microsupercapacitors. *Sustain. Energy Fuels* **2021**, *5* (5), 1235−1254.

(15) Morozov, S. V.; Novoselov, K. S.; Katsnelson, M. I.; Schedin, F.; Elias, D. C.; Jaszczak, J. A.; Geim, A. K. Giant intrinsic carrier mobilities in graphene and its bilayer. *Phys. Rev. Lett.* **2008**, *100* (1), 016602.

(16) Janavika, K. M.; Thangaraj, R. P. Graphene and its application: A review. *Mater. Today Proc.* **2023**.

(17) Si, C.; Sun, Z.; Liu, F. Strain engineering of graphene: a review. *Nanoscale* **2016**, *8* (6), 3207−3217.

(18) Sayed, S.; Gamil, M.; El-Bab, A. F.; Nakamura, K.; Tsuchiya, T.; Tabata, O.; El-Moneim, A. A. Graphene film development on flexible

substrate using a new technique: temperature dependency of gauge factor for graphene-based strain sensors. *Sens. Rev.* **2016**, *36* (2), 140−147.
(19) Gamil, M.; Nageh, H.; Bkrey, I.; El-Moneim, A. A. Graphene-Based strain gauge on a flexible substrate. *Sensor. Mater.* **2014**, *26*, 699−709.
(20) Gamil, M.; Tabata, O.; Nakamura, K.; El-Bab, A. M. F.; Abd El-Moneim, A. Investigation of a new high sensitive Micro-Electro-mechanical strain gauge sensor based on graphene piezoresistivity. *Key Eng. Mater.* **2014**, *605*, 207−210.
(21) Kang, D. J.; Lee, K. H.; Noh, S. H.; Shin, H.; Jeong, W.; Lee, H.; Seo, Y.; Han, T. H. Impermeable graphene skin increases the heating efficiency and stability of an MXENE heating element. *Small* **2023**, *19* (44), 2301077.
(22) Li, Y.; Ai, Q.; Mao, L.; Guo, J.; Gong, T.; Lin, Y.; Wu, G.; Huang, W.; Zhang, X. Hybrid strategy of graphene/carbon nanotube hierarchical networks for highly sensitive, flexible wearable strain sensors. *Sci. Rep.* **2021**, *11* (1), 21006.
(23) Mao, L.; Pan, T.; Guo, J.; Ke, Y.; Zhu, J.; Cheng, H.; Lin, Y. Reconfigurable, Stretchable Strain Sensor with the Localized Controlling of Substrate Modulus by Two-Phase Liquid Metal Cells. *Nanomaterials* **2022**, *12* (5), 882.
(24) Lin, J.; Peng, Z.; Liu, Y.; Ruiz-Zepeda, F.; Ye, R.; Samuel, E. L. G.; Yacaman, M. J.; Yakobson, B. I.; Tour, J. M. Laser-induced porous graphene films from commercial polymers. *Nat. Commun.* **2014**, *5* (1), 5714.
(25) Yu, H.; Gai, M.; Liu, L.; Chen, F.; Bian, J.; Huang, Y.; Yu, C.; Production, F. Laser-induced direct graphene patterning: from formation mechanism to flexible applications. *Soft Sci.* **2023**, *3* (1), 4.
(26) Velasco, A.; Ryu, Y. K.; Hamada, A.; de Andrés, A.; Calle, F.; Martinez, J. Laser-Induced Graphene Microsupercapacitors: Structure, quality, and performance. *Nanomaterials* **2023**, *13* (5), 788.
(27) Carvalho, A. F.; Fernandes, A. J. S.; Leitão, C.; Deuermeier, J.; Marques, A. C.; Martins, R.; Fortunato, E.; Costa, F. M. Laser-Induced Graphene strain sensors produced by ultraviolet irradiation of polyimide. *Adv. Funct. Mater.* **2018**, *28* (52), 1805271.
(28) Tiliakos, A.; Ceaus, C.; Iordache, S. M.; Vasile, E.; Stamatin, I. Morphic transitions of nanocarbons via laser pyrolysis of polyimide films. *J. Anal. Appl. Pyrolysis* **2016**, *121*, 275−286.
(29) Wang, H.; Zhao, Z.; Liu, P.; Guo, X. A soft and stretchable electronics using laser-induced graphene on polyimide/PDMS composite substrate. *npj Flexible Electron.* **2022**, *6* (1), 26.
(30) Kwon, S.; Jung, D.; Lim, H.; Kim, G.; Choi, K.-B.; Lee, J. Laser-assisted selective lithography of reduced graphene oxide for fabrication of graphene-based out-of-plane tandem microsupercapacitors with large capacitance. *Appl. Phys. Lett.* **2017**, *111* (14), 143903.
(31) Mao, L.; Gong, T.; Ai, Q.; Hong, Y.; Guo, J.; He, Y.; Huang, W.; Yu, B. Morphologically modulated laser-patterned reduced graphene oxide strain sensors for human fatigue recognition. *Smart Mater. Struct.* **2020**, *29* (1), 015009.
(32) Tao, L.-Q.; Tian, H.; Liu, Y.; Ju, Z.-Y.; Pang, Y.; Chen, Y.-Q.; Wang, D.-Y.; Tian, X.-G.; Yan, J.-C.; Deng, N.-Q.; Yang, Y.; Ren, T.-L. An intelligent artificial throat with sound-sensing ability based on laser induced graphene. *Nat. Commun.* **2017**, *8* (1), 14579.
(33) Yen, Y.-H.; Hsu, C.-S.; Lei, Z.-Y.; Wang, H.-J.; Su, C.-Y.; Dai, C.-L.; Tsai, Y.-C. Laser-Induced Graphene Stretchable Strain Sensor with Vertical and Parallel Patterns. *Micromachines* **2022**, *13* (8), 1220.
(34) Rahimi, R.; Ochoa, M.; Yu, W.; Ziaie, B. Highly stretchable and sensitive unidirectional strain sensor via laser carbonization. *ACS Appl. Mater. Interfaces* **2015**, *7* (8), 4463−4470.
(35) Kaidarova, A.; Kosel, J. Physical sensors Based on Laser-Induced Graphene: A review. *IEEE Sensor. J.* **2021**, *21* (11), 12426−12443.
(36) Luo, S.; Hoang, P. T.; Liu, T. Direct laser writing for creating porous graphitic structures and their use for flexible and highly sensitive sensor and sensor arrays. *Carbon* **2016**, *96*, 522−531.
(37) Wang, Y.; Wang, L.; Yang, T.; Li, X.; Zang, X.; Zhu, M.; Wang, K.; Wu, D.; Zhu, H. Wearable and highly sensitive graphene strain sensors for human motion monitoring. *Adv. Funct. Mater.* **2014**, *24* (29), 4666−4670.
(38) Liu, M.; Sun, J.; Chen, Q. Influences of heating temperature on mechanical properties of polydimethylsiloxane. *Sens. Actuators, A* **2009**, *151* (1), 42−45.
(39) SYLGARD 184 Silicone Elastomer Kit. https://www.dow.com/es-es/pdp.sylgard-184-silicone-elastomer-kit.01064291z.html#overviewaccessed 6th March 2023.
(40) Zhang, S.; Ge, C.; Liu, R. Mechanical characterization of the stress-strain behavior of the polydimethylsiloxane (PDMS) substate of wearable strain sensors under uniaxial loading conditions. *Sens. Actuators, A* **2022**, *341*, 113580.
(41) Kaidarova, A.; Khan, M. A.; Marengo, M.; Swanepoel, L.; Przybysz, A.; Muller, C.; Fahlman, A.; Buttner, U.; Geraldi, N. R.; Wilson, R. P.; Duarte, C. M.; Kosel, J. Wearable multifunctional printed graphene sensors. *npj Flexible Electron.* **2019**, *3* (1), 15.
(42) Huang, L.; Wang, H.; Wu, P.; Huang, W.; Gao, W.; Fang, F.; Cai, N.; Chen, R.; Zhu, Z. Wearable flexible strain sensor based on Three-Dimensional wavy Laser-Induced graphene and silicone rubber. *Sensors* **2020**, *20* (15), 4266.
(43) Liu, W.; Huang, Y.; Peng, Y.; Walczak, M.; Wang, D.; Chen, Q.; Liu, Z.; Li, L. Stable wearable strain sensors on textiles by direct laser writing of graphene. *ACS Appl. Nano Mater.* **2020**, *3* (1), 283−293.
(44) Kim, T. K.; Kim, J. K.; Jeong, O. C. Measurement of nonlinear mechanical properties of PDMS elastomer. *Microelectron. Eng.* **2011**, *88* (8), 1982−1985.
(45) Tian, H.; Shu, Y.; Cui, Y.-L.; Mi, W.-T.; Yang, Y.; Xie, D.; Ren, T.-L. Scalable fabrication of high-performance and flexible graphene strain sensors. *Nanoscale* **2014**, *6* (2), 699−705.
(46) Lamberti, A.; Perrucci, F.; Caprioli, M.; Serrapede, M.; Fontana, M.; Bianco, S.; Ferrero, S.; Tresso, E. New insights on laser-induced graphene electrodes for flexible supercapacitors: tunable morphology and physical properties. *Nanotechnology* **2017**, *28* (17), 174002.
(47) Abdulhafez, M.; Tomaraei, G. N.; Bedewy, M. Fluence-Dependent morphological transitions in Laser-Induced graphene electrodes on polyimide substrates for flexible devices. *ACS Appl. Nano Mater.* **2021**, *4* (3), 2973−2986.
(48) De La Roche, J.; López-Cifuentes, I.; Jaramillo-Botero, A. Influence of lasing parameters on the morphology and electrical resistance of polyimide-based laser-induced graphene (LIG). *Carbon Lett.* **2023**, *33* (2), 587−595.
(49) Wang, W.; Lu, L.; Li, Z.; Xie, Y. Laser induced 3D porous graphene dots: Bottom-up growth mechanism, multi-physics coupling effect and surface wettability. *Appl. Surf. Sci.* **2022**, *592*, 153242.
(50) Paillet, M.; Parret, R.; Sauvajol, J.-L.; Colomban, P. Graphene and related 2D materials: An overview of the Raman studies. *J. Raman Spectrosc.* **2018**, *49* (1), 8−12.
(51) Cong, X.; Liu, X.-L.; Lin, M.-L.; Tan, P.-H. Application of Raman spectroscopy to probe fundamental properties of two-dimensional materials. *npj 2D Mater. Appl.* **2020**, *4* (1), 13.
(52) Liu, K.; Yang, C.; Zhang, S.; Wang, Y.; Zou, R.; Alamusi, N.; Deng, Q.; Hu, N. Laser direct writing of a multifunctional superhydrophobic composite strain sensor with excellent corrosion resistance and Anti-Icing/Deicing performance. *Mater. Des.* **2022**, *218*, 110689.
(53) Cheng, L.; Fang, G.; Wei, L.; Gao, W.; Wang, X.; Lv, Z.; Xu, W.; Ding, C.; Wu, H.; Zhang, W.; Liu, A. Laser-Induced Graphene strain sensor for conformable Lip-Reading recognition and Human-Machine interaction. *ACS Appl. Nano Mater.* **2023**, *6* (9), 7290−7298.
(54) Ferrari, A. C.; Robertson, J. Interpretation of Raman spectra of disordered and amorphous carbon. *Phys. Rev. B: Condens. Matter Mater. Phys.* **2000**, *61* (20), 14095−14107.
(55) Ni, Z.; Wang, Y.; Yu, T.; Shen, Z. Raman spectroscopy and imaging of graphene. *Nano Res.* **2008**, *1* (4), 273−291.
(56) Wu, J.-B.; Lin, M.-L.; Cong, X.; Liu, H.-N.; Tan, P.-H. Raman spectroscopy of graphene-based materials and its applications in related devices. *Chem. Soc. Rev.* **2018**, *47* (5), 1822−1873.

https://doi.org/10.1021/acsomega.3c09067
ACS Omega 2024, 9, 38359−38370

(57) Chen, H.; Zhuo, F.; Zhou, J.; Liu, Y.; Zhang, J.; Dong, S.; Liu, X.; Elmarakbi, A.; Duan, H.; Fu, Y. Advances in graphene-based flexible and wearable strain sensors. *Chem. Eng. J.* **2023**, *464*, 142576.
(58) Li, Y.; Jia, W.; Hou, X.; Zhang, L.; He, J.; Mu, J.; Wang, C.; Yu, J.; Bi, K.; Cui, M.; Wang, X.; Chou, X. Enhanced-sensitivity and highly flexible stress/strain sensor based on PZT nanowires-modified graphene with wide range carrier mobility. *J. Mater. Sci. Mater. Electron.* **2020**, *31* (11), 8436−8445.
(59) BF120 10AA 120 Ohm Strain Gauge High-Precision Resistance Foil Strain Gauge, Weldable Strain Gauge Surface Strain Gauge Circuit (BF120−10AA): Amazon.com: Industrial & Scientific. https://www.amazon.com/High-Precision-Resistance-Gauge%EF%BC%8CWeldable-Surface-BF120-10AA/dp/B09LV4K86P/ref=sr_1_2?crid=3Q3ZU12S0RM9E&keywords=BF120%2B10AA%2Bstrain%2Bgauge&qid=1705274292&sprefix=bf120%2B10aa%2Bstrain%2Bgauge%2Caps%2C244&sr=8-2&th=1accessed 10th January 2024.
(60) A Series & U series Transducer strain gauges; HBM. https://www.hbm.com/fr/8277/a-and-u-series-transducer-strain-gauges/?product_type_no=A%20Series%20&%20U%20Series%20Transducer%20Strain%20Gaugesaccessed 10th January 2024.
(61) DigChip IC database. https://www.digchip.com/datasheets/parts/datasheet/3375/CEA-06-125UN-350.phpaccessed 10th January 2024.
(62) Ramírez, J.; Urbina, A. D.; Kleinschmidt, A. T.; Finn, M.; Edmunds, S. J.; Esparza, G. L.; Lipomi, D. J. Exploring the limits of sensitivity for strain gauges of graphene and hexagonal boron nitride decorated with metallic nanoislands. *Nanoscale* **2020**, *12* (20), 11209−11221.

https://doi.org/10.1021/acsomega.3c09067
ACS Omega 2024, 9, 38359−38370